JOURNAL OF AIRCRAFT
Vol. 39, No. 2, March–April 2002

Comparison of Wing Characteristics at an Ultralow Reynolds Number

S. Sunada*
Osaka Prefecture University, Osaka 599-8531, Japan
T. Yasuda† and K. Yasuda‡
Nihon University, Chiba 274-8501, Japan
and
K. Kawachi§
University of Tokyo, Tokyo 153-8904, Japan

The hydrodynamic characteristics of 20 wings of different airfoil shape were measured at $Re = 4 \times 10^3$. Each wing had an aspect ratio AR of 7.25. Comparison of the measured wing characteristics showed that hydrodynamic characteristics of a wing with a rectangular airfoil can be improved by either a camber of 5%, a sharp leading edge, or proper corrugation.

Nomenclature

AR	=	geometrical aspect ratio, b/c
a_0	=	two-dimensional lift curve slope by Eq. (4)
$\bar{a}_0$	=	lift curve slope estimated by Eq. (6)
b	=	span length
C_D, C_L	=	drag and lift coefficients of a three-dimensional wing
$C_D(C_L = 0)$	=	three-dimensional drag coefficient at $C_L = 0$
C_d, C_ℓ	=	drag and lift coefficients of a two-dimensional wing
$C_d(C_\ell = 0)$	=	two-dimensional drag coefficient at $C_\ell = 0$
$\bar{C}_d(C_\ell = 0)$	=	drag coefficient at $C_\ell = 0$ estimated by Eq. (10)
$C_{L\alpha}$	=	three-dimensional lift curve slope
$\lvert C_L/C_D\rvert_{\max}$	=	maximum lift–drag ratio of a three-dimensional wing
c	=	chord length
F_X, F_Z	=	hydrodynamic forces acting on both a wing and a connecting cylinder in X and Z directions
F_{X0}, F_{Z0}	=	hydrodynamic forces acting on a connecting cylinder in X and Z directions
f/c	=	maximum camber, in percentage of the chord
h	=	height of corrugation
L_X, L_Y, L_Z	=	dimensions of water tank
Re	=	Reynolds number, $V_0 c/\nu$
t	=	thickness of a wing
t_m	=	mean thickness of a wing
V_0	=	forward velocity of a wing
X, Y, Z	=	fixed coordinate system of a wing
x_f/c	=	location of maximum camber, in percentage of the chord from the leading edge
α	=	angle of attack
α_0	=	zero-lift angle of attack
Δ_n	=	coefficient of the angle of attack given by Eq. (2)
δ_b	=	clearance between wing and bottom of the water tank
δ_n	=	coefficient of the angle of attack given by Eq. (5)
$\bar{\delta}_n$	=	coefficient of the angle of attack estimated by Eqs. (8) and (9)
δ_w	=	clearance between wing and water surface
ν	=	kinematic viscosity of water
ρ	=	density of water
σ	=	Prandtl–Glauert factor for induced drag
τ	=	Prandtl–Glauert factor for induced angle of attack
ϕ	=	particle diameter of iron powder on a wing

Received 22 February 2001; revision received 2 November 2001; accepted for publication 12 November 2001.

*Associate Professor, Department of Aerospace Engineering, Graduate School of Engineering; sunada@aero.osakafu-u.ac.jp.
†Graduate Student, Department of Aerospace Engineering, College of Science and Technology.
‡Associate Professor, Department of Aerospace Engineering, College of Science and Technology. Senior Member AIAA.
§Professor, Research Center for Advanced Science and Technology. Associate Fellow AIAA.

Introduction

THE performance of airfoils operating at a Reynolds number of $Re \approx 10^5$ has been of interest for various applications, including remotely piloted vehicles, sailplanes, and human-powered vehicles.[1] Much research has been done on the performance of airfoils at $Re \approx 10^5$ and it has revealed a large difference in airfoil characteristics between $Re > 10^6$ and $Re \approx 10^5$. Recently, the Defense Advanced Research Projects Agency in the United States proposed developing a small insectlike flying machine.[2–4] Wings of centimeter-sized flying machines operate at $10^3 < Re < 10^5$. Wing characteristics at $10^4 < Re < 10^5$ have been extensively investigated,[5] whereas those at $10^3 < Re < 10^4$ (Refs. 6 and 7) have not. Sunada et al.[8,9] conducted two systematic studies on wing characteristics at $Re = 4 \times 10^3$ by measuring the wing characteristics, and Kunz and Kroo[10] did a systematic study on airfoil characteristics at $10^3 < Re < 10^4$ by using computational fluid dynamics. These three systematic studies showed that thin airfoils having about 5% camber ratio have a high lift–drag ratio at $10^3 < Re < 10^4$. This airfoil shape is similar to that investigated by the Wright brothers (see Ref. 11) for developing a glider, whose wing operates at $Re > 10^6$.

In the measurements by Sunada et al.,[8] a part of each wing was in water, as shown in Fig. 1a. The measured hydrodynamic characteristics of the wings included both a three-dimensional effect due to the finite aspect ratio AR and a wave drag due to the wave generated on the water surface. In the study, the finite aspect ratio of 7.25 was as large as possible for the experimental apparatus, such that this three-dimensional effect was minimized. Our current study expands the previous study by Sunada et al.[8] as follows.

1) The hydrodynamic forces, not including the wave drag, acting on a wing with AR = 7.25 were measured.

2) The hydrodynamic forces were measured for additional airfoil shapes with corrugation and a sharp leading edge and for airfoil

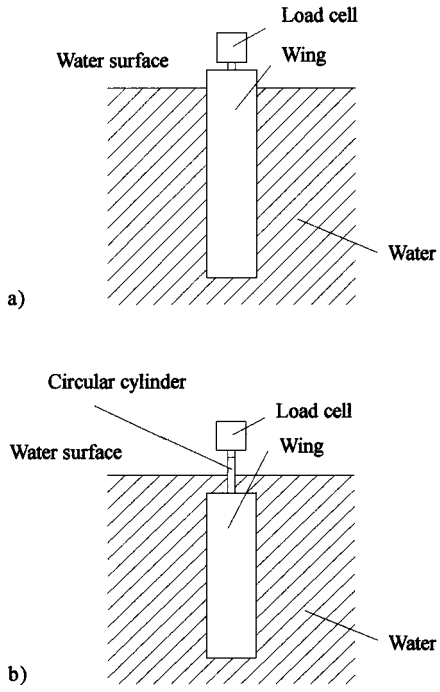

Fig. 1 Part of wing submerged in water during force measurements: a) in the previous experiments by Sunada et al.[8] and b) in the present experiments.

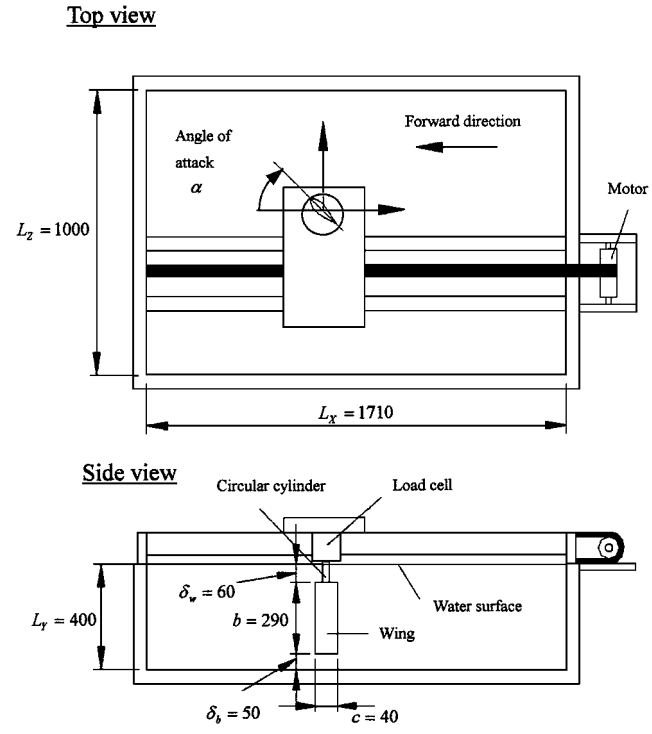

Fig. 2 Experimental apparatus used to measure three-dimensional hydrodynamic forces.

shapes included in the previous study by Sunada et al.[8] The effects of corrugation and a sharp leading edge on the hydrodynamic characteristics of wings were, thus, clarified.

3) The hydrodynamic forces acting on a wing were measured for various aspect ratios to clarify the three-dimensional effect on the wing characteristics.

Experiments

Materials and Methods

The experimental apparatus used to measure the hydrodynamic forces on the wings is shown in Fig. 2. The 20 wings, whose airfoils are shown in Fig. 3, were towed through water in a tank ($L_X = 1710$ mm, $L_Z = 1000$ mm, and $L_Y = 400$ mm). Of these airfoils, 14 were studied previously by Sunada et al.,[8] and 6 (airfoils 4, 6–8, 19, and 20) are newly studied here. All of the wings had a chord length $c = 40$ mm, a span length $b = 290$ mm, and an aspect ratio $AR = b/c = 7.25$.

The wings were connected to a load cell via a 8-mm-diam cylinder as shown in Fig. 1b, and then the forces exerted on the wing and the cylinder were measured as each wing was moved through the water in the tank. As discussed later in this section, this connecting cylinder moving through the water allows the hydrodynamic forces acting only on the wing to be measured, and thus, those forces that do not include the wave drag can be determined. For comparison, Fig. 1a shows the configuration used in the previous study by Sunada et al.,[8] where the wave drag acting on the wing was included in the hydrodynamic characteristics.

In the water tank, the wing velocity rapidly reached a constant velocity of $V_0 = 0.12$ m/s, within 1 s. Therefore, the Reynolds number $Re = V_0 c/\nu$ was 4×10^3. The load cell measured the hydrodynamic forces in the X and Z directions, F_X and F_Z, respectively, which are composed of forces acting on the wing and on the cylinder in water.

The same measurement was made without the wing to obtain the hydrodynamic forces acting on the cylinder in water in the X and Z directions, F_{X0} and F_{Z0}, respectively. When it is assumed that the interference effect between the wing and the cylinder is negligible, the hydrodynamic forces acting on the wing in the X and Z directions are $F_X - F_{X0}$ and $F_Z - F_{Z0}$, respectively. From these

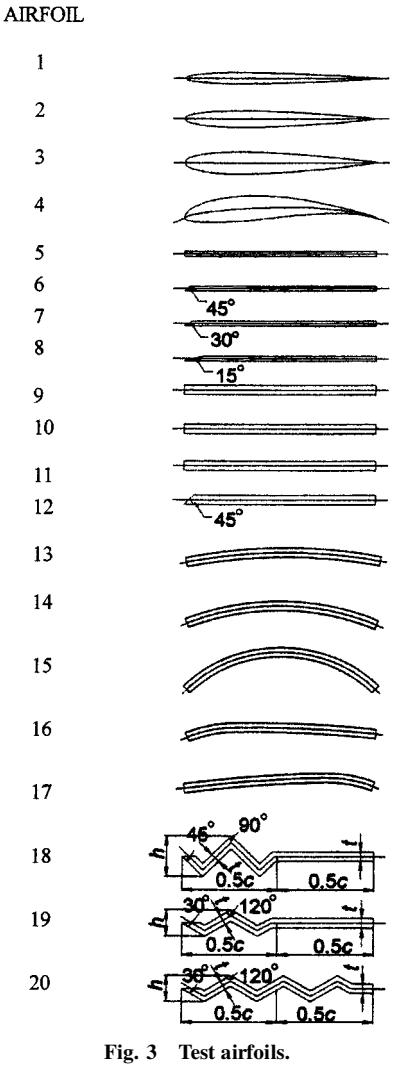

Fig. 3 Test airfoils.

forces, the lift and drag force coefficients, C_L and C_D, respectively, can be determined:

$$C_L = \frac{F_Z - F_{Z0}}{0.5\rho V_0^2 bc}, \qquad C_D = \frac{F_X - F_{X0}}{0.5\rho V_0^2 bc} \tag{1}$$

In our experiments, the interference effect between the side walls of the tank and the wing was negligible because the size of the water tank ($L_X = 1710$ mm and $L_Z = 1000$ mm) was much larger than the chord length c. On the other hand, the interference effect between the wing and the water surface and that between the wing and the bottom of the water tank were not expected to be negligible because the clearance between the wing and the bottom of the water tank was $\delta_b = 60$ mm and that between the wing and the surface of the water was $\delta_w = 50$ mm and because δ_b/b and δ_w/b both were about 0.2. However, because we expected these interference effects on the wing characteristics to be comparable for all of the wings studied here, these effects did not affect the comparisons of the obtained wing characteristics.

For all wings in general, when α is smaller than their stall angle, C_D can be approximated as follows:

$$C_D = C_D(C_L = 0) + \Delta_1(\alpha - \alpha_0) + \Delta_2(\alpha - \alpha_0)^2 \tag{2}$$

For some wings, when α is close to 0 deg, C_L can be approximated as follows:

$$C_L = C_{L\alpha}(\alpha - \alpha_0) \tag{3}$$

Experimental Uncertainty

The bias errors were due mainly to the load cell and strain amplifier. The maximum bias error was less than 5%. The precision error was mainly due to the angle-of-attack measurement, the wing velocity measurement, and the disturbance resulting from the wing motion. This error produced scatter in the C_L and C_D data, resulting in an error of 5%.

The total measurement errors from these two sources in C_L and C_D were, therefore, $\approx\sqrt{(5^2 + 5^2)}$, less than 8%. These errors were small enough relative to the differences in characteristics of the airfoils that they were ignored.

Results and Discussion

Figures 4–15 show the α–C_L and α–C_D curves and the effect of airfoil shape on the wing characteristics. Table 1 gives the data of the airfoils' shapes, and Table 2 lists the measured wing characteristics.

Thickness Ratio

The effect of thickness ratio on the wing characteristics can be shown for three groups of airfoils: streamlined shape (airfoils 1–3), flat plates (airfoils 5 and 9), and flat plates with a sharp leading edge (airfoils 6 and 12). For all three groups, $|C_L/C_D|_{\max}$ increased as the mean thickness ratio t_m/c decreased. The differences in $|C_L/C_D|_{\max}$ among airfoils 1–3 are mainly caused by differences in the α–C_L curves (Fig. 4a), whereas the difference between airfoils 5 and 9 and that between airfoils 6 and 12 are mainly caused by differences in the α–C_D curves (Fig. 5b).

Streamlined Shape

The effect of streamlined shape on the wing characteristics was studied for three airfoils with streamlined shape (airfoils 1–3) and a flat plate (airfoil 9). Based on the t_m/c for airfoil 1 (3.8%) and that for airfoil 2 (5.7%), the α–C_L and α–C_D curves for a NACA00 series airfoil with $t_m/c = 5\%$ (not studied here) were expected to be between the curves for airfoil 1 and airfoil 2 as shown in Fig. 4. These estimated C_L and C_D for this NACA00 series airfoil are smaller than those for airfoil 9, which is a flat plate having the same t_m/c (Fig. 5). Based on the measured $|C_L/C_D|_{\max}$ for airfoils 1–3, the estimated $|C_L/C_D|_{\max}$ for this NACA00 series airfoil is 5.6. When this value was compared with that for airfoil 9 having the same t_m/c, the streamlined airfoil had larger $|C_L/C_D|_{\max}$ than did a rectangular airfoil.

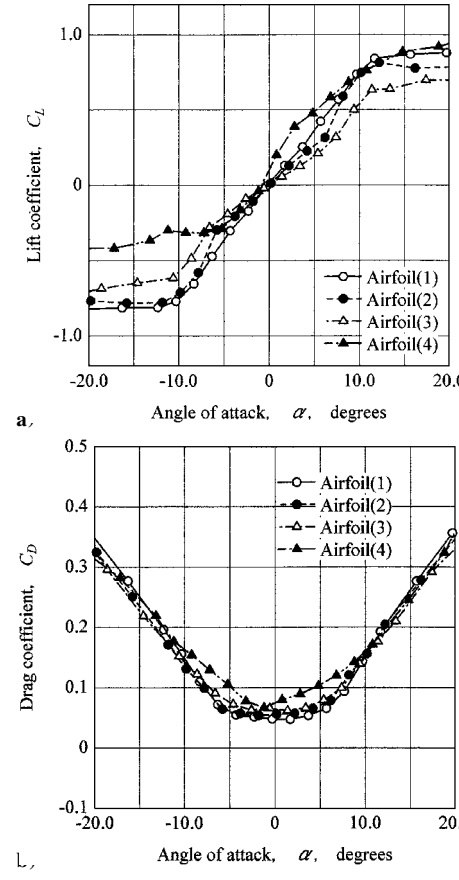

Fig. 4 Effect of streamlined shape on a) lift coefficient and b) drag coefficient of three-dimensional wings.

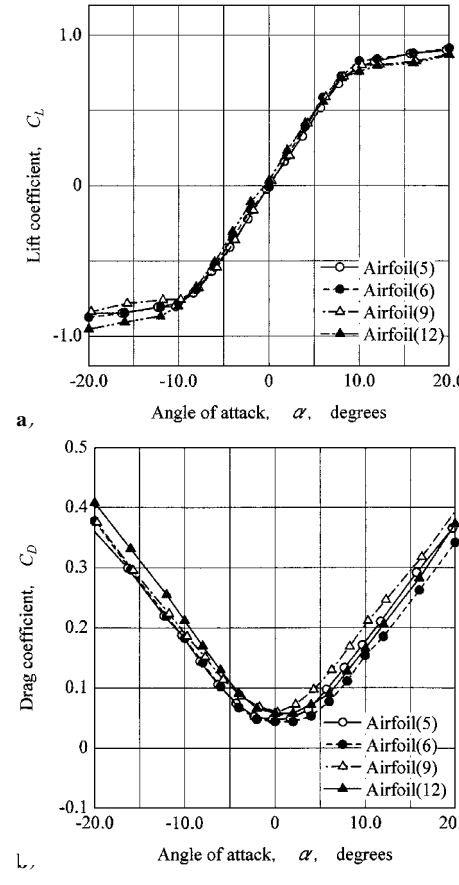

Fig. 5 Effect of a sharp leading edge and thickness ratio on a) lift coefficient and b) drag coefficient of three-dimensional wings.

Table 1 Airfoil shape data

Airfoil no.	Mean thickness ratio t_m/c, %	Maximum camber ratio f/c, %	Location of maximum camber x_f/c, %	Height of corrugation h/c, %	Remarks
1	3.8	0	——	——	NACA0006
2	5.7	0	——	——	NACA0009
3	7.6	0	——	——	NACA0012
4	7	6	53		Wortmann FX63-137
5	2.5	0	——	——	
6	2.5	0	——	——	
7	2.4	0	——	——	
8	2.4	0	——	——	
9	5	0	——	——	
10	5	0	——	——	Iron powder ($\phi = 15\mu$) on the surface
11	5	0	——	——	Iron powder ($\phi = 30\mu$) on the surface
12	4.9	0	——	——	
13	5	5	50	——	Circular arc
14	5	10	50	——	Circular arc
15	5	20	50	——	Circular arc
16	5	5	25	——	Two circular arcs are connected at 25% chordwise position
17	5	5	75	——	Two circular arcs are connected at 75% chordwise position
18	5	——	——	14	Corrugated airfoil
19	5	——	——	14	Corrugated airfoil
20	5	——	——	22	Corrugated airfoil

Table 2 Wing characteristics

Airfoil no.	$C^{a}_{L\alpha}$	$C_D(C_L=0)$	Δ_1	Δ_2	$\lvert(C_L/C_D)_{\max}\rvert(\alpha$ deg)
1	4.3	0.044	−0.015	2.8	6.7 (7)
2	——	0.054	0.052	1.5	5.0 (8)
3	——	0.059	0.006	2.8	4.1 (10)
4	——	0.067	−0.014	2.9	4.9 (7)
5	5.1	0.045	0.004	4.8	5.4 (6)
6	5.2	0.041	−0.11	4.4	7.9 (6)
7	5.1	0.041	−0.17	4.1	8.5 (6)
8	5.0	0.040	−0.24	3.8	9.4 (6)
9	5.4	0.064	0.020	5.0	4.5 (7)
10	5.4	0.059	0.062	5.7	4.9 (7)
11	5.4	0.065	0.084	4.8	5.1 (5)
12	5.0	0.066	−0.16	4.7	6.4 (6)
13	——	0.10	−0.016	3.2	6.4 (7.5)
14	——	0.13	0.022	2.7	5.2 (7.5)
15	——	0.20	0.16	3.1	3.1 (13.5)
16	——	0.093	−0.44	3.0	7.6 (6.5)
17	——	0.097	0.34	4.3	5.9 (3.5)
18	——	0.18	−0.24	1.1	3.3 (11)
19	5.1	0.090	−0.13	2.9	5.1 (6)
20	——	0.093	−0.13	2.4	4.4 (9)

[a]Values were obtained only when the relation between α and C_L at small angles of attack is linear.

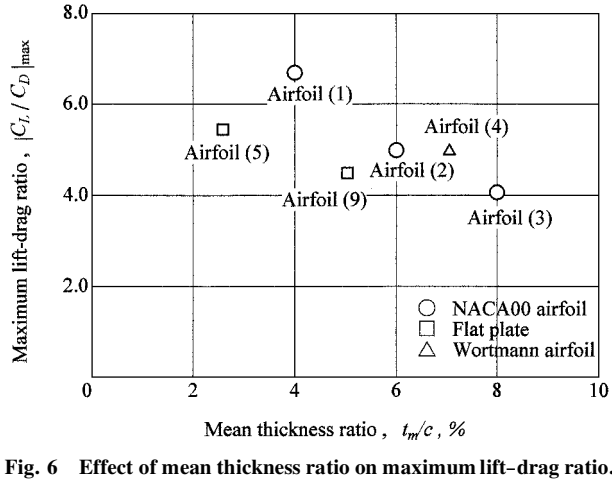

Fig. 6 Effect of mean thickness ratio on maximum lift–drag ratio.

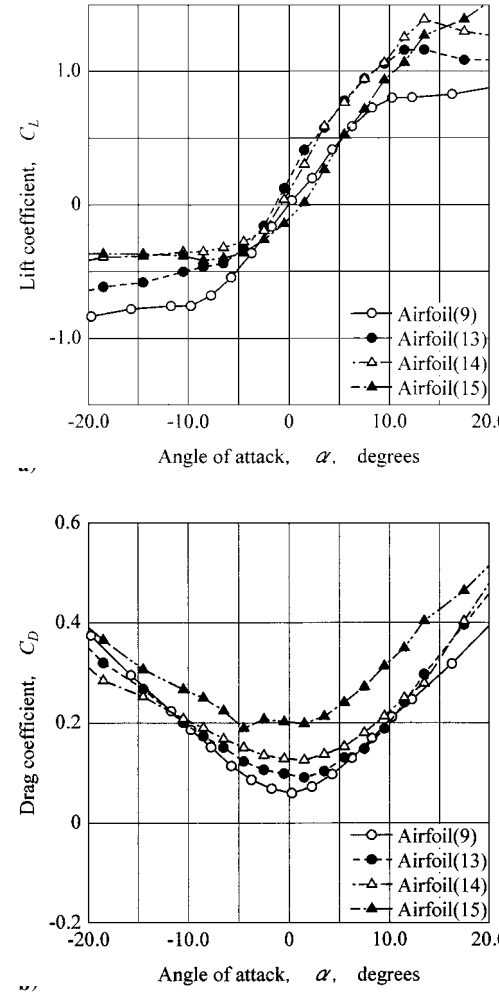

Fig. 7 Effect of maximum camber ratio on the a) lift coefficient and b) drag coefficient of three-dimensional wings.

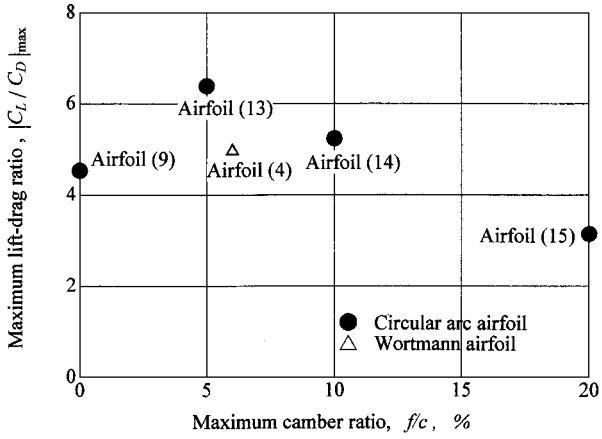

Fig. 8 Effect of maximum camber ratio on maximum lift–drag ratio.

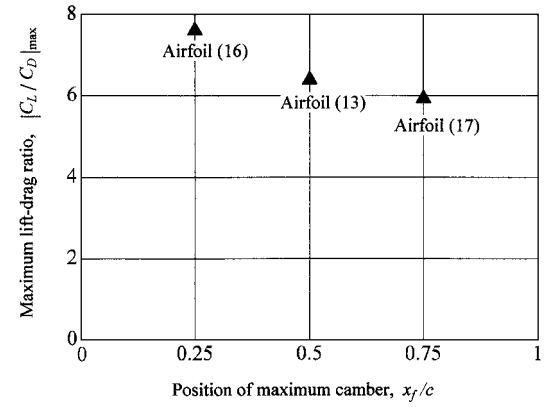

Fig. 10 Effect of position of maximum camber on maximum lift–drag ratio.

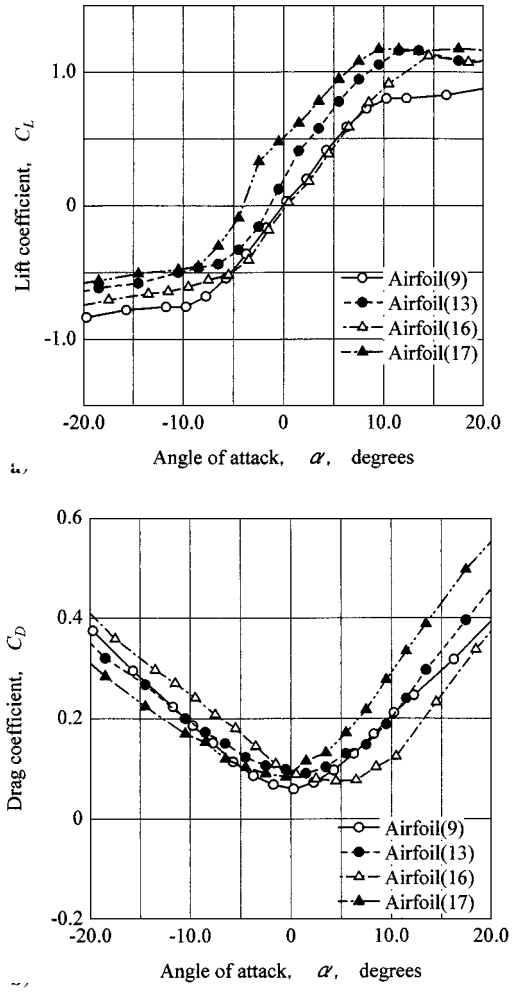

Fig. 9 Effect of position of maximum camber on a) lift coefficient and b) drag coefficient of three-dimensional wings.

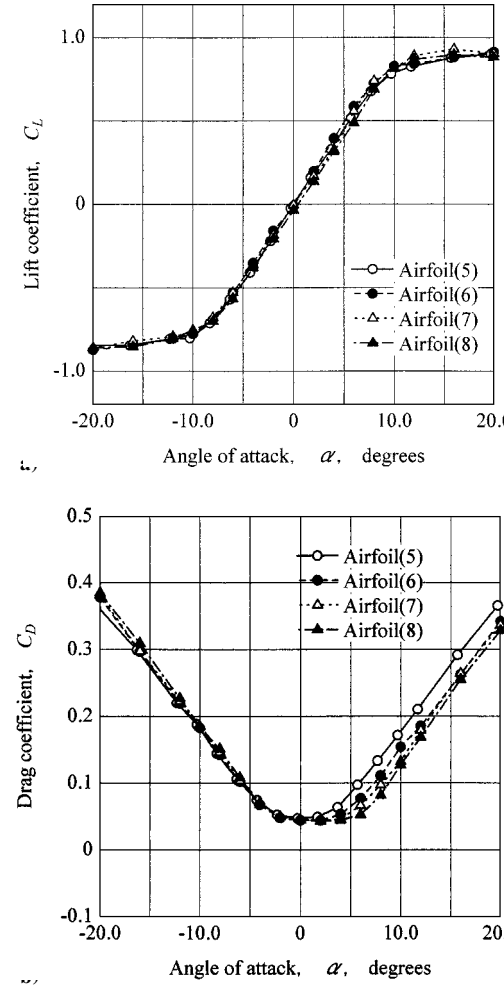

Fig. 11 Effect of a sharp leading edge on a) lift coefficient and b) drag coefficient of three-dimensional wings.

Camber Ratio

The effect of camber ratio on the wing characteristics was studied for four circular arc airfoils (airfoils 9 and 13–15). Comparison of measured C_L among these airfoils shows that C_L was largest when the camber ratio f/c was either 5 or 10% (Fig. 7). Comparison of C_D among these airfoils shows that C_D increased when the f/c was increased and when $-10\,\text{deg} < \alpha < 10\,\text{deg}$. These results show that, for these four airfoils, the $|C_L/C_D|_{max}$ was maximum when f/c was 5% (Fig. 8).

Position of Maximum Camber

The effect of the position of maximum camber on the wing characteristics was studied for three airfoils (airfoils 13, 16, and 17) that have $f/c = 5\%$. Comparison of C_L among these airfoils shows that C_L increased as the position of the maximum camber approached the trailing edge, that is, as x_f/c was increased (Fig. 9). Comparison of C_D shows that when $\alpha > 0$, the C_D decreased as x_f/c was decreased. Conversely, when $\alpha < 0$, the C_D increased as x_f/c was decreased. Comparison of $|C_L/C_D|_{max}$ (Fig. 10) shows that $|C_L/C_D|_{max}$ was maximum when the position of the maximum camber was at the 25% chordwise position, that is, $x_f/c = 0.25$.

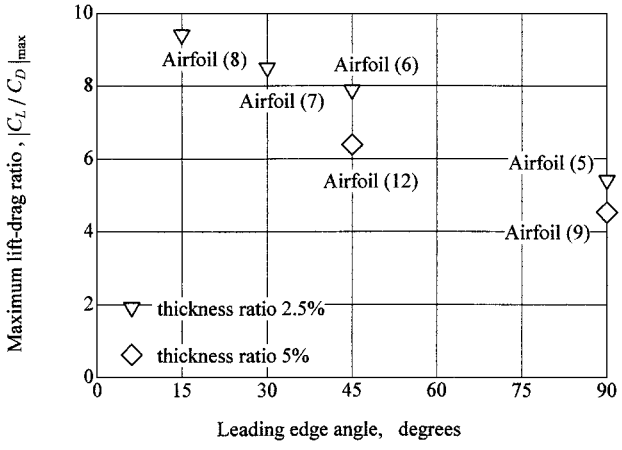

Fig. 12 Effect of leading-edge angle on maximum lift–drag ratio.

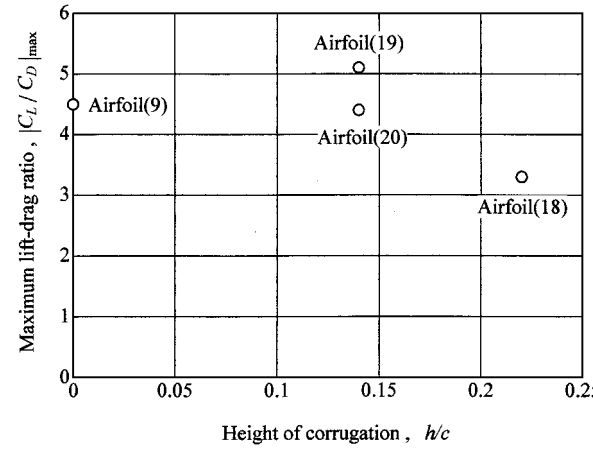

Fig. 14 Effect of corrugation height on maximum lift–drag ratio.

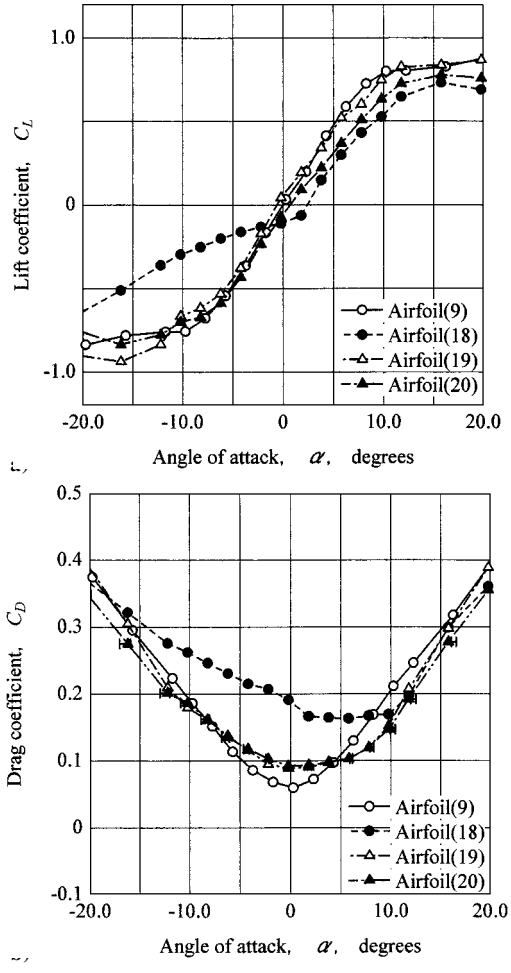

Fig. 13 Effect of corrugation on a) lift coefficient and b) drag coefficient of three-dimensional wings.

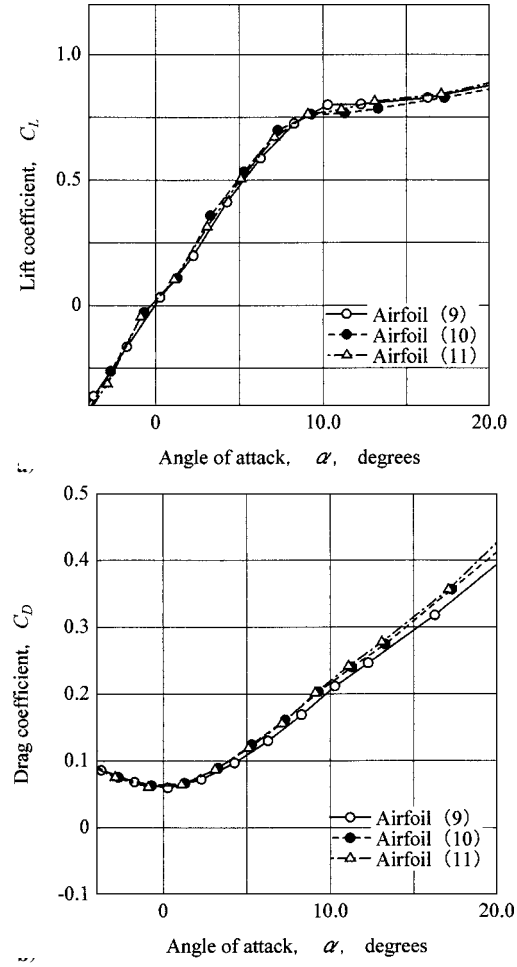

Fig. 15 Effect of roughness on a) lift coefficient and b) drag coefficient of three-dimensional wings.

Wortmann FX 63-137 Airfoil

Based on $|C_L/C_D|_{max}$ for airfoils 1–3, (Fig. 6), the estimated $|C_L/C_D|_{max}$ for a NACA00 series airfoil with $t_m/c = 7\%$ is 4.4. Comparison of this estimated $|C_L/C_D|_{max}$ with that measured for airfoil 4 having the same t_m/c shows that airfoil 4, which is a typical airfoil at $Re \approx 10^5$, had larger $|C_L/C_D|_{max}$ than did this NACA00 series airfoil. The reason for the larger $|C_L/C_D|_{max}$ is that airfoil 4 is cambered ($f/c > 0$).

Based on $|C_L/C_D|_{max}$ for airfoils 9 and 13–15 shown in Fig. 8, the estimated $|C_L/C_D|_{max}$ is 6.0 for a circular arc airfoil with $f/c = 6\%$. Comparison of this estimated $|C_L/C_D|_{max}$ with that measured for airfoil 4 having the same f/c shows that airfoil 4 had smaller $|C_L/C_D|_{max}$ than did the circular arc airfoil having the same f/c. This smaller $|C_L/C_D|_{max}$ is because the mean thickness ratio of airfoil 4 ($t_m/c = 7\%$) is larger than that of airfoils 9 and 13–15 ($t_m/c = 5\%$) and because a thinner wing has larger $|C_L/C_D|_{max}$ as discussed earlier. Note that $x_f/c \approx 50\%$ for airfoils 4, 9, and 13–15.

Angle of Leading Edge

Comparison of $|C_L/C_D|_{max}$ for airfoils 5–8 and that for airfoils 9 and 12 in Fig. 12 shows that $|C_L/C_D|_{max}$ increased as the angle of the leading edge was decreased. The sharper leading edge increased the $|C_L/C_D|_{max}$. The differences in $|C_L/C_D|_{max}$ among airfoils 5–8

and those between airfoils 9 and 12 are mainly caused by differences in the α–C_D curves, as shown in Fig. 11b and Fig. 5b, respectively.

Corrugation

Comparison of $|C_L/C_D|_{\max}$ among airfoils 9 and 18–20 in Fig. 14 shows that only the $|C_L/C_D|_{\max}$ of airfoil 19 was larger than that of airfoil 9, which is a flat plate. This means that proper corrugation increases the lift–drag ratio. Note that $t_m/c \approx 5\%$ for airfoils 9 and 18–20. The difference in $|C_L/C_D|_{\max}$ between airfoils 9 and 19 is mainly caused by differences in the α–C_D curves in Fig. 13b.

Roughness

Comparison of C_L and C_D for airfoils 9–11, in Fig. 15 shows that the effect of roughness on wing characteristics was small.

Flow Visualization

Sunada et al.[8,9] did flow visualization around airfoils 3–6, 9, 12, 13, and 19. The water level in the water tank was decreased so that part of the wing was above the water surface. Flow around the wing was visualized by floating aluminum dust on the water surface. Relation between the flow visualization and the measured hydrodynamic forces is as follows.

Airfoils 3, 4, and 13

For airfoils 3, 4, and 13, the separation point was located on the upper surface between the leading and trailing edges, and this point moved toward the leading edge with an increase in the angle of attack. These airfoils experience a so-called trailing-edge stall.[12] Kinks in the α–C_L curves for these wings (Figs. 4a and 7a) occurred at angles of attack smaller than their stall angle.

Airfoils 5, 6, 9, 12, and 19

For airfoils 5, 6, 9, 12, and 19, unsteady vortices were generated at the leading edge. The α–C_L curves for these wings (Fig. 5a), except airfoil 18, have higher linearity than do airfoils 3, 4, and 13.

Summary

The results in the subsections on thickness ratio, streamlined shape, camber ratio, and roughness agree with those obtained by Sunada et al.,[8] whereas the result in the subsection on position of maximum camber differs. In the experiments by Sunada et al.,[8] the $|C_L/C_D|_{\max}$ was maximum when the position of the maximum camber was 50%, compared with the 25% obtained in the present experiments. This difference is caused by the difference in how the wing was mounted to the load cell, as shown in Fig. 1. The results in the subsections on the Wortmann FX 63-137 airfoil, angle of the leading edge, and corrugation are newly obtained results.

Effect of Aspect Ratio on Measured Three-Dimensional Lift and Drag Coefficients

Force measurements for various AR were made to determine the effect of AR on the hydrodynamic forces for various b. Airfoil 8, with $c = 28.8$ mm, was used because, in this discussion, we use potential flow theory where the relation between α and C_L is linear. Note that the relation between α and C_L for airfoil 8 is linear as shown in Fig. 11. The clearance between the wing and the surface of the water was fixed at $\delta_w = 30$ mm and that between the wing and the bottom of the water tank was varied as a function of b, that is, $\delta_b = (370 - b)$ mm. Therefore, the interference effect between the wing and the bottom of the water tank varied as b was varied.

Figure 16 shows the effect of AR on the lift slope $C_{L\alpha}$ in Eq. (3) and on the coefficients Δ_2 and $C_D(C_L = 0)$ in Eq. (2). The $C_{L\alpha}$ at $AR = 7.25$ is smaller than that at $AR > 7.25$. Therefore, the $C_{L\alpha}$ and Δ_2 at $AR = 7.25$ that we measured include a three-dimensional effect. The contribution of this three-dimensional effect in $C_{L\alpha}$ and Δ_2 can be determined by estimating the lift and drag coefficients of

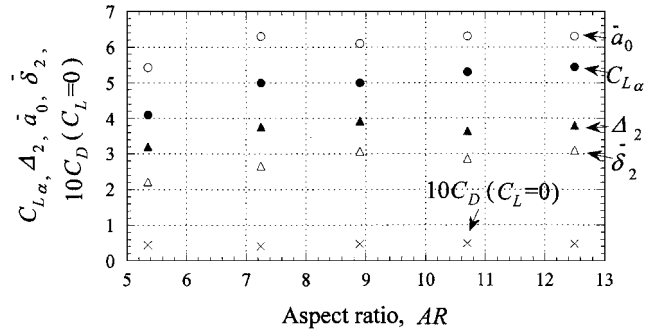

Fig. 16 Effect of AR on the three-dimensional characteristics for airfoil 8.

a two-dimensional airfoil. For this estimate, the lift coefficient and drag coefficient for a two-dimensional airfoil is approximated as

$$C_\ell = a_0(\alpha - \alpha_0) \tag{4}$$

$$C_d = C_d(C_\ell = 0) + \delta_1(\alpha - \alpha_0) + \delta_2(\alpha - \alpha_0)^2 \tag{5}$$

Then, the four coefficients, a_0, $C_d(C_\ell = 0)$, δ_1, and δ_2, in Eqs. (4) and (5) are obtained as follows: The values of $\bar{a}_0$ and $\bar{C}_d$, that is, $\bar{C}_d(C_\ell = 0)$, $\bar{\delta}_1$ and $\bar{\delta}_2$, are estimated from measured $C_{L\alpha}$ and Δ_2 as

$$\bar{a}_0 = \frac{C_{L\alpha}}{1 - (C_{L\alpha}/\pi AR)(1 + \tau)} \tag{6}$$

$$\bar{C}_d \equiv \bar{C}_d(C_\ell = 0) + \bar{\delta}_1(\alpha - \alpha_0) + \bar{\delta}_2(\alpha - \alpha_0)^2$$

$$= C_D - \left(C_L^2/\pi AR\right)(1 + \sigma) \tag{7}$$

Equations (2), (5), and (7) become

$$\bar{\delta}_2 = \Delta_2 - \left(C_{L\alpha}^2/\pi AR\right)(1 + \sigma) \tag{8}$$

$$\bar{\delta}_1 = \Delta_1 \tag{9}$$

$$\bar{C}_d(C_\ell = 0) = C_D(C_L = 0) \tag{10}$$

The values of τ and σ approach 0 (Ref. 13) when $AR > 5$, assuming the interference effect between the wing and the bottom of the water tank and that between the wing and the water surface are negligible. Because it is not yet clear how τ and σ are affected by these interference effects, which are varied by AR, the following discussion we assumed $\tau, \sigma = 0$.

The measured $C_D(C_L = 0)$ in Fig. 16 are independent of AR, and the constant value is $\bar{C}_d(C_\ell = 0)$, as indicated by Eq. (10). Because the term $\bar{\delta}_1\alpha$, that is, $\bar{\delta}_1\alpha$, is much smaller than the other terms in Eq. (5), $\bar{\delta}_1$ will not be discussed here. The parameters a_0 and δ_2 correspond to asymptotic limits $\bar{a}_0$ and $\bar{\delta}_2$ with increasing AR. The estimated a_0 and δ_2 are 6.2 and 3, respectively, from $\bar{a}_0$ and $\bar{\delta}_2$ shown in Fig. 16. The $C_{L\alpha}$ and Δ_2 at $AR = 7.25$ differ from the estimated a_0 and δ_2 by about 30%. Such a large three-dimensional effect might be included in the wing characteristics that we measured.

Laitone[14,15] showed that potential flow theory is not valid for wing/airfoil characteristics at $Re < 5 \times 10^5$ for two reasons. The first reason is that certain wings with $AR \approx 6$ have $C_{L\alpha}$ larger than the two-dimensional lift slope 2π determined by using potential flow theory. The second reason is that, when the drag coefficient of a wing with finite aspect ratio is approximated by $C_D = C_D(C_L = 0) + \Delta_2(\alpha - \alpha_0)^2$, induced drag $\Delta_2(\alpha - \alpha_0)^2$ is much larger than $(C_L^2/\pi AR)(1 + \sigma)$ (Ref. 14) estimated by using potential flow theory. However, why Eqs. (6) and (7) are not valid for wing/airfoil characteristics at $Re = 4 \times 10^3$ remains unclear. Furthermore, when induced drag is assumed to be $(\Delta_2 - \delta_2)(\alpha - \alpha_0)^2$ as indicated by Eq. (8), the second reason stated might disappear. Therefore, the values of a_0 and δ_2 were just reference data.

Conclusions

Hydrodynamic characteristics were measured for 20 wings with $AR = 7.25$. Because of the experimental method shown in Fig. 1b, these characteristics did not include the effect of wave drag, which was included in previous experiments by Sunada et al.[8] When the effect of wave drag is removed, our results show that the maximum camber position is at the 25% chordwise position for wings with arc airfoils having camber ratio of 5% for maximum $|C_L/C_D|_{\max}$.

Our results also show that hydrodynamic characteristics of a wing having a rectangular airfoil can be improved by either a camber of 5%, a sharp leading edge, or proper corrugation. Corrugation is particularly effective in improving the wing characteristics better for the following reasons. Previous studies[8,9] as well as our current study show that a thinner wing has better hydrodynamic characteristics. However, a thinner wing has lower rigidity. When the thinner wing cannot support the pressure because of lower rigidity, corrugation is effective. This is because corrugation makes the thinner wing stronger against the bending moment and the torsional moment when an airfoil is thin and the warping is restricted. Therefore, a thinner wing with corrugation has high hydrodynamic characteristics and high rigidity. This is probably why insects' wings are thin and have corrugation.

Acknowledgment

This research was financially supported by the Research and Development Applications of Advanced Computational Science and Technology of the Japan Science and Technology Corporation.

References

[1]Gad-el-Hak, M., "Control of Low-Speed Airfoil Aerodynamics," *AIAA Journal*, Vol. 28, No. 9, 1990, pp. 1537–1552.

[2]Morris, S. J., and Holden, M., "Design of Micro Air Vehicles and Flight Test Validation," *Proceedings of the Conference on Fixed, Flapping and Rotary Vehicles at Very Low Reynolds Numbers*, edited by T. J. Mueller, Univ. of Notre Dame, Notre Dame, IN, 2000, pp. 153–175.

[3]Kroo, I., and Kunz, P. J., "Meso-Scale Flight and Miniature Rotorcraft Development," *Proceedings of the Conference on Fixed, Flapping and Rotary Vehicles at Very Low Reynolds Numbers*, edited by T. J. Mueller, Univ. of Notre Dame, Notre Dame, IN, 2000, pp. 184–196.

[4]Pornsin-Sirirak, T. N., Lee, S. W., Nassef, H., Grasmeyer, J., Tai, Y. C., Ho, C. M., and Keennon, M., "MEMS Wing Technology for a Battery-Powered Ornithopter," *Proceedings of the IEEE Micro Electronics Mechanical Systems 2000*, Inst. of Electrical and Electronics Engineers, New York, 2000, pp. 799–804.

[5]Schmitz, F. W., "Aerodynamics of the Model Airplane. Part I. Airfoil Measurements," NACA TM X-60976, 1967.

[6]Jensen, M., "Biology and Physics of Locust Flight. III. The Aerodynamics of Locust Flight," *Philosophical Transactions of the Royal Society of London*, Ser. B, Vol. 239, 1956, pp. 511–552.

[7]Kesel, A. B., "Aerodynamic Characteristics of Dragonfly Wing Sections Compared with Technical Aerofoils," *Journal of Experimental Biology*, Vol. 203, 2000, pp. 3125–3135.

[8]Sunada, S., Sakaguchi, A., and Kawachi, K., "Airfoil Section Characteristics at a Low Reynolds Number," *Journal of Fluids Engineering*, Vol. 119, March 1997, pp. 129–135.

[9]Sunada, S., Yasuda, T., Yasuda, K., Kawachi, K., Ozaki, K., and Tanaka, T., "Airfoil Characteristics at a Low Reynolds Number," *Journal of Flow Visualization and Image Processing*. Vol. 7, No. 2, 2000, pp. 123–131.

[10]Kunz, P. J., and Kroo, I., "Analysis, Design, and Testing of Airfoils for Use at Ultra-Low Reynolds Numbers," *Proceedings of the Conference on Fixed, Flapping and Rotary Vehicles at Very Low Reynolds Numbers*, edited by T. J. Mueller, Univ. of Notre Dame, Notre Dame, IN, 2000, pp. 349–372.

[11]Anders, J. D., Jr., *A History of Aerodynamics*, Cambridge Univ. Press, Cambridge, England, U.K., 1997, Chap. 5.

[12]Gault, D. E., "A Correlation of Low-Speed, Airfoil-Section Stalling Characteristics with Reynolds Number and Airfoil Geometry," NACA TN 3963, 1957.

[13]Jacobs, E. N., and Abbott, I. H., "The NACA Variable-Density Wind Tunnel," NACA Rept. 416, 1932.

[14]Laitone, E. V., "Wind Tunnel Tests of Wings at Reynolds Numbers Below 70,000," *Experiments in Fluids*, Vol. 23, 1997, pp. 405–409.

[15]Laitone, E. V., "Wind Tunnel Tests of Wings at Reynolds Numbers Below 70,000," *AIAA Journal*, Vol. 34, No. 9, 1997, pp. 1941, 1942.